Crystal Growth

DOI: 10.1002/anie.201210329

Calcite Crystal Growth by a Solid-State Transformation of Stabilized Amorphous Calcium Carbonate Nanospheres in a Hydrogel**

*Assaf Gal, Wouter Habraken, Dvir Gur, Peter Fratzl, Steve Weiner, and Lia Addadi**

During the process of crystal growth, building blocks are added to the crystal lattice. These building blocks may be soluble ions, nanometer-sized prenucleation clusters,[1] or even larger crystallites that undergo oriented attachment.[2] The growth process may affect crystal shape, so that rather than atomically flat facets, aggregations of discrete units (so-called mesocrystals) may form.[3,4] Crystals can also grow via an initial highly disordered phase through a solid-phase amorphous-to-crystalline transition.[5] The differentiation of these crystal-growth mechanisms is challenging, since the building blocks might be very small, short-lived, and unstable.

Some organisms use a transient amorphous precursor phase to build their mature crystalline mineral phase.[6] These biominerals display an amazing variety of detailed morphologies and are often characterized by curved surfaces, occluded additives, and conchoidal fracturing.[7] It was demonstrated in several biological systems that amorphous nanospheres undergo secondary nucleation on the crystalline phase to create a morphology reminiscent of aggregated spheres.[8] This crystal-growth mechanism was observed only in living organisms, which makes its study inseparable from the cellular context.

In this study, we investigated an in vitro induced amorphous-to-crystalline transition that exploits a biogenically produced amorphous calcium carbonate (ACC) phase. The biogenic ACC minerals that we used are produced by plant leaves and are called cystoliths (Figure 1 A).[9,10] The cystolith mineral phase is predominantly ACC, with a minor silica component.[9] The ACC is stable inside the leaf, and when extracted it remains stable at ambient temperature as long as water is completely eliminated from the environment, for example, in a desiccator or in ethanol. Cystoliths show a conchoidal-fracture surface resembling glass (Figure 1 B). The basic building blocks of the cystolith are closely packed nanospheres with a size range of 19.8 ± 3.6 nm, as determined by image analysis (Figure 1 C; see also the Supporting Information). The relative stability and large size of the biogenic ACC nanospheres enabled us to observe the details of a unique transformation mechanism, which resulted in highly ordered single crystals of calcite that are predominantly composed of nanospheres.

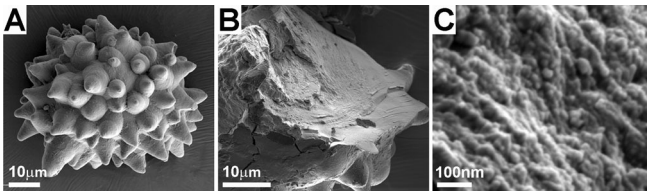

Figure 1. SEM images of cystoliths. A) A single cystolith after extraction from the leaf. B) A fractured cystolith showing conchoidal cleavage, characteristic of amorphous materials. C) High-magnification image of the fracture surface showing the ACC nanospheres that compose the cystolith.

To study the transformation of cystolith ACC into calcite, we placed cystoliths (3 mg) in double-distilled water (DDW; 200 μL) at room temperature. The reaction was quenched after different time periods by removing the water and replacing it with ethanol. Since ACC is more soluble than calcite,[11] the cystolith ACC dissolved until the concentration of ions in the solution exceeded saturation with respect to calcite precipitation. Subsequently, calcite crystals nucleated and grew from the saturated solution. When the process was quenched after 10 min, the cystoliths showed etched surfaces from which partially disaggregated nanospheres and small calcite crystals emerged (Figure 2 A,B). The calcite crystals at this stage were small and were delimited by flat and smooth {104} faces. This surface morphology is characteristic of crystalline calcite that has grown by ion-by-ion accretion from a solution of calcium and carbonate ions.

When the reaction was quenched after 20 min, the calcite crystals on the cystolith surface were larger, as expected after a longer reaction time, but their crystal morphology had changed. In addition to the smooth {104} faces, a new set of partially developed prismatic {*hk*0} faces had formed (Figure 2 C). The topography of these higher-energy surfaces was rough and was found to consist of aggregated particles of the same size as the original ACC nanospheres (Figure 2 D). This change in morphology indicates a change in the dissolution–crystallization process as crystal growth proceeds. In the

[*] A. Gal, D. Gur, Prof. S. Weiner, Prof. L. Addadi
Department of Structural Biology, Weizmann Institute of Science
Rehovot, 76100 (Israel)
E-mail: lia.addadi@weizmann.ac.il
Dr. W. Habraken, Prof. P. Fratzl
Department of Biomaterials
Max Planck Institute of Colloids and Interfaces
14424 Potsdam (Germany)

[**] We thank Dr. Eugenia Klein for her help with the ESEM experiments, and Dr. Stefan Siegel and Dr. Chenghao Li for their help with the diffraction experiments. X-ray diffraction studies were conducted at the μ-Spot beamline of the BESSY II Synchrotron Radiation Facility, which is part of the Helmholtz-Zentrum Berlin für Materialien und Energie. The research was supported by a German Research Foundation grant within the framework of the Deutsch–Israelische Projektkooperation DIP. L.A. is the incumbent of the Dorothy and Patrick Gorman Professorial Chair of Biological Ultrastructure, and S.W. of the Dr. Trude Burchardt Professorial Chair of Structural Biology.

Supporting information for this article is available on the WWW under http://dx.doi.org/10.1002/anie.201210329.

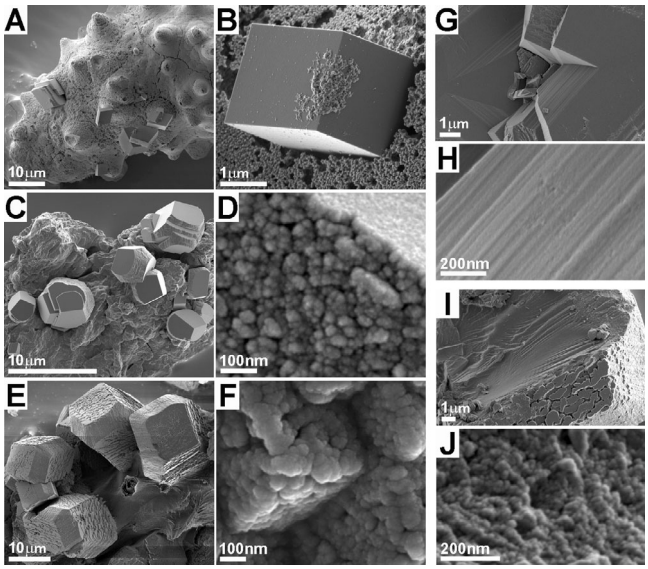

Figure 2. SEM images documenting the aqueous transformation of cystolith ACC into calcite. A) After 10 min in DDW, the cystolith ACC is etched, and small calcite crystals nucleate on its surface. B) Higher-magnification of a calcite crystal. C) After 20 min in DDW, the cystoliths continue to disintegrate; the calcite crystals are larger and express rough {*hk*0} surfaces. D) Higher-magnification image of a crystal showing that nanosphere aggregation forms the rough surface between the smooth {104} faces. E) After 100 min in DDW, the calcite crystals show rough faces, even though the rhombohedral morphology of calcite is conserved. F) At the crystal surface, the nanosphere aggregates form edges and planes according to the crystallographic {104} orientations. G,H) A fracture through the center of a crystal follows {104} cleavage planes. I,J) A fracture through the external layer of a crystal shows conchoidal fracturing and a texture corresponding to nanosphere aggregation.

second phase of crystal growth, the nanospheres from the cystolith ACC migrate and crystallize as discrete entities on the growing calcite crystal. Other components released from the dissolving cystolith substrate probably also interact with the growing crystal surface and thus induce a change in crystal habit.[12]

After 100 min the transformation reaction was complete and all ACC had been consumed by the growing calcite crystals. A few micron-sized crystals were usually found attached to the collapsed organic scaffold of the cystolith (Figure 2E). The crystal surfaces were composed of irregularly pitted {104} faces and partially developed {*hk*0} faces. Close examination of the {104} faces showed that the complete crystal surface consisted of an agglomeration of particles with sizes similar to those of the nanospheres of the original ACC (Figure 2F). This surface texture stands in contrast to the smooth faces of the primarily formed calcite crystals and implies that the ongoing growth of the calcite crystals occurs through particle accretion.

When the resulting calcite crystals are fractured, typical {104} cleavage planes of calcite are exposed at their center (Figure 2G,H). The sharp cleavage planes, however, grade into conchoidal-fracture surfaces close to the outer surface of the crystal (Figure 2I). At higher magnification, the conchoidal fracture still shows the nanosphere morphology of what is now a calcite crystal (Figure 2J).

When control experiments were carried out with synthetic ACC that contained no additives, the resulting calcite crystals showed flat faces without any trace of nanospheres, as expected from ion-by-ion crystal growth (see Figure S1 in the Supporting Information). This difference between the synthetic and biogenic ACC implies that some constituent (or constituents) of the cystolith ACC is responsible for the different crystal-growth mechanism.

We monitored the process of the transformation of ACC into calcite in situ inside an environmental scanning electron microscope (ESEM). Cystoliths were placed in the ESEM, and the water-vapor pressure inside the ESEM chamber was increased so that water condensed on the sample holder and covered the cystoliths. To observe the sample, we reduced the pressure periodically to below the dew point so that liquid water evaporated; in this way, imaging in a high-humidity atmosphere was possible.

When cystoliths were left overnight covered with water inside the ESEM, aggregates of crystals formed and surrounded the original location of a cystolith (Figure 3A). Although the faces of the crystals were discernible, the entire aggregate was unexpectedly covered by a smooth, featureless substance (Figure 3A,B). This substance persisted below the dew point of water, but over time shrank and finally collapsed into a flexible film when the humidity was further decreased (see Figure S2). These properties are characteristics of a hydrogel, which in this case originated from inside the cystolith.

Cystoliths contain polysaccharides that consist mainly of cellulose and pectin.[13] Our analyses showed that the organic fraction of the cystolith is 5% w/w, and infrared spectra confirmed the presence of abundant polysaccharides (see Figures S4 and S5). Amino acid analysis showed that serine-rich proteins comprise only 2% w/w of the organic fraction (see the Supporting Information). Therefore, it is plausible that the obtained hydrogel is mainly composed of cellulose and pectins, which in other plant tissues also exhibit gel-like behavior.[14]

Close examination of the crystals showed that the crystal faces grew around former cystolith components (Figure 3B). The growing terraces had an undulating shape, and the granular morphology of the crystal matched the nanospheres

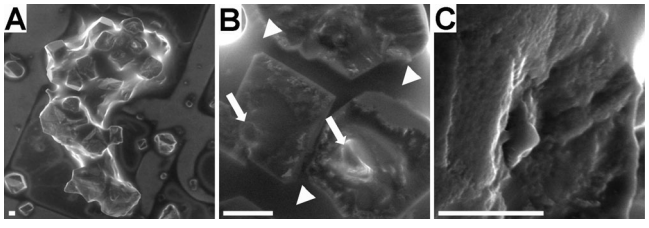

Figure 3. ESEM images of a cystolith undergoing transformation into calcite. A) Gel covering an aggregate of calcite crystals produced from a transforming cystolith. B) Higher magnification of two crystals forming around protrusions in the original cystolith (indicated with arrows). The featureless gel surrounding the crystals is marked by arrowheads. C) Surface of a growing crystal showing the granular morphology of nanosphere aggregation. Scale bars: 10 μm.

identified in the dry crystals (Figure 3C). These observations also show that late-stage crystal growth occurs by the accretion of nanospheres on the existing calcite crystal surface.

The calcite crystals formed by cystolith crystallization were analyzed by microspot X-ray diffraction (micro-XRD). Diffraction patterns were collected using a 10 μm beam diameter from calcite crystals that were isolated from transformed cystoliths. Each rhombohedral-shaped calcite crystal produced a sharp diffraction pattern (Figure 4A). We analyzed the shape of the diffraction spots by measuring the width of the peak in the radial direction and in the azimuthal direction (Figure 4B–D). The strongest {104} diffraction peaks from 10 different crystals had an average radial full width at half maximum (FWHM) of $q = 0.062 \pm 0.017\ nm^{-1}$ and an azimuthal FWHM of $0.27 \pm 0.08°$. These characteristics are similar to those of simultaneously analyzed geogenic crystals, which exhibited a radial FWHM of $q = 0.069 \pm 0.016\ nm^{-1}$ and azimuthal FWHM of $0.24 \pm 0.06°$. The calculated instrumental resolution for the beamline setup used for the measurements was $q = 0.062\ nm^{-1}$. We thus conclude that the FWHM was determined by the instrumental resolution rather than by the crystal quality. This conclusion is consistent with previous reports of calcite crystals with much narrower diffraction-peak widths.[15]

The peak broadening in the radial direction is correlated to the lattice coherence length in the crystal (the size of perfectly ordered crystalline domains) by the Scherrer equation.[16] According to the Scherrer equation, the micro-XRD setup resolution cannot resolve coherence lengths larger than about 170 nm (see the Supporting Information). The results therefore show that the coherence length in the crystals formed from cystoliths is larger than 170 nm and thus at least 8–9 times the size of the nanospheres in the cystolith ACC. The peak broadening in the azimuthal direction indicates the degree of mosaicity in the crystal (the misalignment of perfectly ordered domains). The similarity between this broadening in the geogenic and cystolith-derived calcites shows that both have similar domain alignments. The extended lattice order shows that the cystolith-derived crystals are not a semioriented assembly of previously crystallized ACC nanospheres, but that the particles are transformed upon contact with the crystal surface; in this way, they become structurally fully integrated into the growing crystal at the atomic level. The alternative scenario, in which each nanosphere disaggregates, crystallizes independently, and undergoes oriented attachment to the growing crystal, would result in a reduction of the coherence length to the size of the individual crystallite, as observed in synthetic calcite crystals,[17] and is therefore rejected.

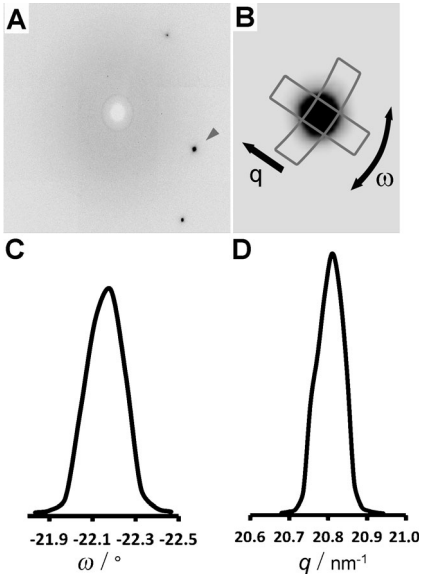

Figure 4. Micro-XRD of a crystal formed by the disaggregation and crystallization of cystolith ACC. A) Diffraction pattern of an isolated crystal. The intensity scale is inverted for better visualization of the diffraction spots. B) Detailed image of a single (104) diffraction spot marked by the arrowhead in (A). C,D) Example of diffraction-spot analysis: azimuthal profile (C) and radial profile (D) of the rectangles shown on the diffraction spot in (B).

The calcite growth process described herein provides mechanistic insight into the crystallization pathway that starts with ACC nanospheres. In the case of synthetic ACC, the ACC dissolved into ions, and the calcite crystals grew by the adsorption of these ions on their surfaces, as deduced from the smoothness of their facets. In contrast, the calcite crystals formed from biogenic stabilized ACC clearly showed an initial ion-by-ion growth followed by a shift to an accretion process via nanospheres that did not dissolve. The fact that the coherence lengths of the formed crystals are much longer than the diameters of the nanospheres demonstrates that the amorphous nanospheres undergo secondary nucleation on the crystal surface; this process results in a seamless continuity of the crystal lattice. Interestingly, the parts of the crystals that formed through nanosphere crystallization displayed a conchoidal fracture as opposed to the atomically flat cleavage of the parts that formed by ion adsorption.

We do not know what attributes of the cystoliths are responsible for stabilizing the nanospheres in such a way that they can adsorb directly on the crystal surface without dissolving. The quantity of inorganic additives, such as magnesium and silicate ions, in the cystoliths is so low that such species are unlikely to account for the nanosphere stability.[18] When the cystoliths were completely dissolved into ions with acid, and carbonate was reintroduced by diffusion into the solution, only ion-by-ion crystal growth was observed (see Figure S3). Also in experiments in which the transformation of synthetic ACC that was precipitated in the presence of purified organic components of the cystoliths was tested, only ion-by-ion crystal growth was observed (see Figure S3). These control experiments demonstrate that the original organization and microenvironment of the nanospheres inside the cystolith are somehow responsible for their enhanced stability, and this stability cannot be reproduced by combining the cystolith components in vitro.

Two mechanisms influence the outcome of the crystallization process: ion-mediated dissolution and precipitation, and nanosphere disaggregation from the cystolith body, followed by nanosphere nucleation on the crystal surface. The prevailing process at the beginning of the transformation is the ion-mediated mechanism, which leads to the character-

istic flat rhombohedral-shaped crystals. With time, the dominant process becomes the nanosphere-mediated mechanism, which results in the nanosphere texture of the rhombohedral-shaped crystals. The whole process, including the transition from one mechanism to the other, is regulated by both kinetics and thermodynamics. The thermodynamic driving force for the formation of calcite after ACC dissolution is the higher solubility of ACC relative to that of calcite; nonetheless, it is conceivable that compositional inhomogeneities within the biogenic composite material could be responsible for the initial dissolution of the cystoliths into ions and the subsequent growth by the addition of more stable particles, as well as of ions from the solution. The resulting morphology reflects the unique balance between nanosphere accretion and ion adsorption. The two competing processes have been thoroughly analyzed for magnetite precipitation from solution.[19]

Mineral growth inside a gel phase was reported to occur in the formation of a few biogenic minerals and might be a widespread mechanism.[20,21] Crystals grown in gels have crystallographic facets and incorporate to some degree the gel-forming molecules.[4,21] Although in cystoliths no crystallization occurs in vivo, the organic scaffold of the cystolith is observed to form a gel phase when crystallization is artificially induced in water. The gel phase around the forming crystals probably limits the nanosphere diffusion in solution and creates a microenvironment that makes the crystallization process very different from equilibrated-solution-mediated growth. Because the nature of this crystal-growth pathway appears to involve "kinetic competition" between the dissolution–precipitation of ions and the disintegration–crystallization of nanospheres, the gel may play a crucial role in controlling diffusion and balancing the relative rates of these processes.

The unique crystallization process of cystoliths leaves many questions open for further investigation. Is there a chemical moiety that prevents the ACC nanospheres from dissolving? Is the reaction environment inside the hydrogel the controlling factor? What are the prevailing thermodynamic and kinetic forces that determine the number, size, and morphology of the calcite crystals, including the coalescence of the nanospheres to form crystallographic planes and edges? Finally, does this solid-state transformation of nanospheres occur in some biological processes in which mature crystals form via a disordered precursor phase?

Received: December 28, 2012
Revised: March 7, 2013
Published online: April 4, 2013

Keywords: amorphous calcium carbonate · biomineralization · crystal growth · cystoliths · X-ray microdiffraction

[1] D. Gebauer, A. Völkel, H. Cölfen, *Science* **2008**, *322*, 1819; E. M. Pouget, P. H. H. Bomans, J. A. C. M. Goos, P. M. Frederik, G. de With, N. A. J. M. Sommerdijk, *Science* **2009**, *323*, 1455; W. J. E. M. Habraken, J. Tao, L. J. Brylka, F. Heiner, L. Bertinetti, A. S. Schenk, A. Verch, V. Dmitrovic, P. H. H. Bomans, P. M. Frederik, J. Laven, P. van der Schoot, B. Aichmayer, G. de With, J. J. DeYoreo, N. A. J. M. Sommerdijk, *Nat. Commun.* **2013**, *4*, 1507.

[2] J. F. Banfield, S. A. Welch, H. Z. Zhang, T. T. Ebert, R. L. Penn, *Science* **2000**, *289*, 751; D. S. Li, M. H. Nielsen, J. R. I. Lee, C. Frandsen, J. F. Banfield, J. J. De Yoreo, *Science* **2012**, *336*, 1014; H. M. Zheng, R. K. Smith, Y. W. Jun, C. Kisielowski, U. Dahmen, A. P. Alivisatos, *Science* **2009**, *324*, 1309.

[3] R. Q. Song, H. Cölfen, *Adv. Mater.* **2010**, *22*, 1301; H. Cölfen, M. Antonietti, *Angew. Chem.* **2005**, *117*, 5714; *Angew. Chem. Int. Ed.* **2005**, *44*, 5576; H. Tlatlik, P. Simon, A. Kawska, D. Zahn, R. Kniep, *Angew. Chem.* **2006**, *118*, 1939; *Angew. Chem. Int. Ed.* **2006**, *45*, 1905.

[4] R. Kniep, P. Simon, *Angew. Chem.* **2008**, *120*, 1427; *Angew. Chem. Int. Ed.* **2008**, *47*, 1405.

[5] P. Fratzl, F. D. Fischer, J. Svoboda, J. Aizenberg, *Acta Biomater.* **2010**, *6*, 1001.

[6] Y. Politi, T. Arad, E. Klein, S. Weiner, L. Addadi, *Science* **2004**, *306*, 1161; L. Addadi, S. Raz, S. Weiner, *Adv. Mater.* **2003**, *15*, 959; S. Weiner, L. Addadi, *Annu. Rev. Mater. Res.* **2011**, *41*, 21.

[7] F. Nudelman, N. A. J. M. Sommerdijk, *Angew. Chem.* **2012**, *124*, 6686; *Angew. Chem. Int. Ed.* **2012**, *51*, 6582; H. A. Lowenstam, S. Weiner, *On Biomineralization*, Oxford University Press, New York, **1989**.

[8] C. E. Killian, R. A. Metzler, Y. U. T. Gong, I. C. Olson, J. Aizenberg, Y. Politi, F. H. Wilt, A. Scholl, A. Young, A. Doran, M. Kunz, N. Tamura, S. N. Coppersmith, P. U. P. A. Gilbert, *J. Am. Chem. Soc.* **2009**, *131*, 18404; I. Sethmann, G. Worheide, *Micron* **2008**, *39*, 209; L. Addadi, D. Joester, F. Nudelman, S. Weiner, *Chem. Eur. J.* **2006**, *12*, 981; Y. Oaki, H. Imai, *Small* **2006**, *2*, 66; J. Mahamid, A. Sharir, L. Addadi, S. Weiner, *Proc. Natl. Acad. Sci. USA* **2008**, *105*, 12748; J. Seto, Y. R. Ma, S. A. Davis, F. Meldrum, A. Gourrier, Y.-Y. Kim, U. Schilde, M. Sztucki, M. Burghammer, S. Maltsev, C. Jäger, H. Cölfen, *Proc. Natl. Acad. Sci. USA* **2012**, *109*, 3699; Y. Politi, R. A. Metzler, M. Abrecht, B. Gilbert, F. H. Wilt, I. Sagi, L. Addadi, S. Weiner, P. Gilbert, *Proc. Natl. Acad. Sci. USA* **2008**, *105*, 17362.

[9] H. J. Arnott in *The Mechanisms of Biomineralization in Animals and Plants* (Eds.: M. Omori, N. Watabe), Tokai University Press, Tokyo, **1980**, p. 211.

[10] A. Gal, A. Hirsch, S. Siegel, C. H. Li, B. Aichmayer, Y. Politi, P. Fratzl, S. Weiner, L. Addadi, *Chem. Eur. J.* **2012**, *18*, 10262.

[11] L. Brečević, A. E. Nielsen, *J. Cryst. Growth* **1989**, *98*, 504.

[12] L. Addadi, Z. Berkovitch-Yellin, N. Domb, E. Gati, M. Lahav, L. Leiserowitz, *Nature* **1982**, *296*, 21.

[13] W. M. Watt, C. K. Morrell, D. L. Smith, M. W. Steer, *Ann. Bot.* **1987**, *60*, 71.

[14] P. H. Norberg, H. Meier, *Holzforschung* **1966**, *20*, 174; J. R. Barnett, V. A. Bonham, *Biol. Rev.* **2004**, *79*, 461.

[15] A. Berman, L. Addadi, A. Kvick, L. Leiserowitz, M. Nelson, S. Weiner, *Science* **1990**, *250*, 664.

[16] A. Guinier, *X-Ray Diffraction in Crystals, Imperfect Crystals, and Amorphous Bodies*, W. H. Freeman, San Francisco, CA, **1963**.

[17] J. Aizenberg, J. Hanson, T. F. Koetzle, S. Weiner, L. Addadi, *J. Am. Chem. Soc.* **1997**, *119*, 881.

[18] A. Gal, S. Weiner, L. Addadi, *J. Am. Chem. Soc.* **2010**, *132*, 13208.

[19] J. Baumgartner, A. Dey, P. H. H. Bomans, C. Le Coadou, P. Fratzl, N. A. J. M. Sommerdijk, D. Faivre, *Nat. Mater.* **2013**, *12*, 310.

[20] E. Asenath-Smith, H. Y. Li, E. C. Keene, Z. W. Seh, L. A. Estroff, *Adv. Funct. Mater.* **2012**, *22*, 2891.

[21] G. M. Khalifa, S. Weiner, L. Addadi, *Cryst. Growth Des.* **2011**, *11*, 5122; H. Y. Li, H. L. Xin, D. A. Muller, L. A. Estroff, *Science* **2009**, *326*, 1244.

